

Tow waviness and anisotropy effects on Mode II fracture of triaxially woven composite

M.Y. Al-Fasih¹, A.B.H. Kueh^{*1}, S.H. Abo Sabah¹ and M.Y. Yahya²

¹ Construction Research Centre, Faculty of Civil Engineering, Universiti Teknologi Malaysia, 81310 UTM Johor Bahru, Johor, Malaysia

² Centre for Composites, Faculty of Mechanical Engineering, Universiti Teknologi Malaysia, 81310, UTM Johor Bahru, Johor, Malaysia

(Received July 14, 2016, Revised October 6, 2016, Accepted January 11, 2018)

Abstract. Mode II fracture toughness, K_{IIC} , of single-ply triaxially woven fabric (TWF) composite due to tow waviness and anisotropy effects were numerically and experimentally studied. The numerical wavy beam network model with anisotropic material description denoted as TWF anisotropic was first validated with experimental Mode II fracture toughness test employing the modified compact tensile shear specimen configuration. 2D planar Kagome and TWF isotropic models were additionally constructed for various relative densities, crack lengths, and cell size parameters for examining effects due to tow waviness and anisotropy. K_{IIC} generally increased with relative density, the inverse of cell size, and crack length. It was found that both the waviness and anisotropy of tow inflict a drop in K_{IIC} of TWF. These effects were more adverse due to the waviness of tow compared to anisotropy.

Keywords: waviness; anisotropy; fracture toughness; triaxially woven fabric composite; 2D planar

1. Introduction

There is recently an increased interest in using the triaxially woven fabric (TWF) composite in numerous advanced engineering applications that demand lightness and flexibility. These include active and morphing aerospace structures, reinforcing element for automobiles and aircrafts, and filtering system, to name but a few (Baier and Datashvili 2011, Hoa *et al.* 2003, Zhao and Hoa 2005). In a single-ply form, TWF handles load uniformly in both tension and shear as well as bending (Kueh 2012, 2014). Like most fiber reinforced composites, it exhibits good stiffness and strength properties (Kueh 2012, Xu *et al.* 2007) as well as lightweight but greatly flexible in particular in the out-of-plane direction (Aoki *et al.* 2007, Kueh 2013). In addition, it features good impact behavior and has a low thermal sensitivity (Zhao and Hoa 2003). These attractive behaviors are due to its high porosity, which results also in efficient heat dispersion.

Fig. 1 shows a piece of cured TWF composite with three sets of tows, located along 0°, 60°, and -60°-directions from the horizontal axis. Due to such architectural arrangement, one can see on a planar viewpoint a uniformly distributed series of hexagonal voids. These voids result in a reduction in the mass of TWF, an attractive property for lightweight and flexible structure applications. Highlighted in the same figure is the unit cell of TWF with t and l defined as the cell wall thickness and cell size, respectively.

Due to the equal distribution of load-resisting tows in the 0°, 60°, and -60°-directions, this material possesses on

a macroscopic scale a quasi-isotropic behavior, a useful asset for engineering applications, without being burdened by the common design process of laminated composites that requires the stacking sequence consideration.

In the aerospace applications, TWF as the structural component is subjected to numerous intense mechanical and thermal loads, resulting in the Mode I, Mode II, and Mixed mode fractures. These deformation modes demand the understanding of the fracture toughness of TWF, which is defined as the ability of a material to resist the propagation of crack. Despite the significance of the fracture toughness of TWF, it should be noted that there is thus far no study on this important property especially with respect to Mode II loading (Al-Fasih *et al.* 2017). In comparison, there exist numerous studies on fracture properties of other more established materials (Erfani and Akrami 2016, Rizov 2017, Toribio and Ayaso 2003). It is essential to realize that from a two-dimensional perspective although the topology of the single-ply TWF composite resembles that of the planar Kagome lattice, their out-of-plane geometrical features are not identical. This results in some substantial differences in their behaviors. This study aims to explore how their main differences, i.e., waviness and anisotropy, contribute to the change in the fracture toughness, in particular, under the Mode II loading environment.

There is much work, which has revealed extensively the fracture toughness of two-dimensional elastic, brittle, and perfect lattices, employing chiefly the modeling technique (Fleck and Qiu 2007, Lipperman *et al.* 2007). Some essential outcomes are presented next. The main consensus from these studies is that the fracture toughness of lattices increases with relative density. Toughness depends strongly on relative density, weakly on cell size, and proportionally

*Corresponding author, Ph.D.,

E-mail: kbhahmad@utm.my; ak_sibu@yahoo.com

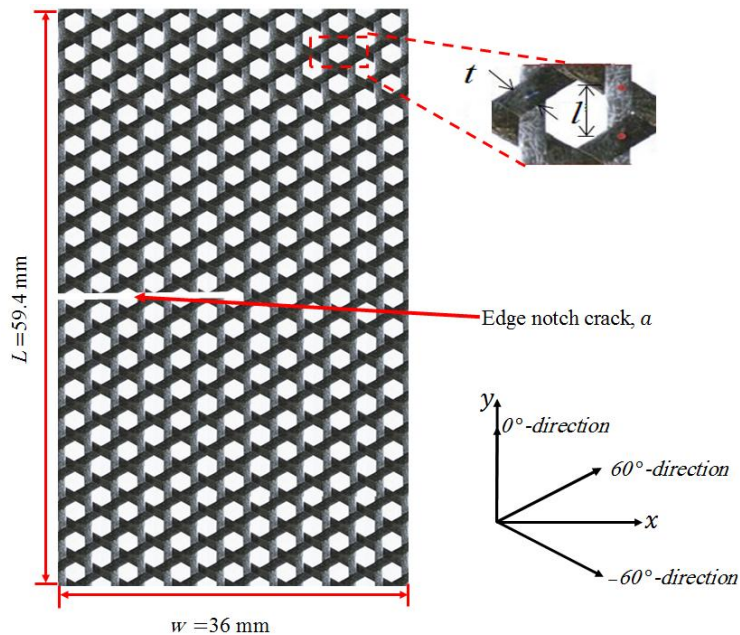


Fig. 1 Compact tensile shear specimen of triaxially woven fabric composite and its highlighted unit cell

on the fracture strength of cell edge material (Romijn and Fleck 2007). It was concluded that the Mode I fracture toughness, K_{IC} , when arranged from the greatest to the lowest, is found in Kagome, triangular-celled, and hexagonal-celled lattices. Also, the deformation mode for the triangular-celled lattice is stretching-dominated; for hexagonal-celled lattice it is bending-dominated, while Kagome is dominated by both stretching and bending. K_{IC} of Kagome lattice is the greatest amongst these lattices because of the appearance of an elastic, bending zone stemming from the crack tip into a remote stretching field. Romijn and Fleck (2007) however discovered that the fracture toughness of Kagome lattice is highly sensitive to imperfection in the form of a random dispersion of the joint position, resulting in the highest knockdown in mechanical properties. To better approach practical scenario, Huang and Gibson (1991b) adopted the finite element model to investigate the effects of short crack and cell wall modulus of rupture that is varied by the Weibull distribution on the fracture toughness of brittle honeycombs. A reduction trend was found in the fracture toughness when the crack length over cell size ratio is less than 7. Weibull modulus of the cell wall material presented a good prediction of the fracture toughness measured in their experiments. Using a similar technique, Huang and Gibson (1991a) then established for brittle foams that when the Weibull modulus is lesser than 6, increase in cell size reduces K_{IC} . The reverse is true when the Weibull modulus is greater than 6. When the Weibull modulus is 6, K_{IC} remains constant. Alonso and Fleck (2009) by means of an analytical model predicted the fracture toughness of an elastic-brittle, diamond-celled lattice with a central crack. They noticed that the linear elastic fracture mechanics applies when the crack length much exceeds the cell size. However, when the crack covers only a few cells, the stress concentration at the crack tip is negligible and the strength rekindles with that of the unnotched. Adopting the micromechanics approach,

Choi and Sankar (2005) and Thiyagasundaram *et al.* (2011) noticed that for high relative densities, K_{IC} of foams with thicker struts is higher than that with thinner struts when both are of the same densities. However, for low densities, this influence was not demonstrated. Lee *et al.* (2007) using the micro- and macro-mechanical finite element models observed that the fracture toughness of homogeneous foam is approximately the same as that of functionally graded when both have the same microstructure and density at the crack tip. Christodoulou and Tan (2013) came to the conclusion that the crack initiation occurs at up to six cells from the crack tip in regions of high strain gradient and high localized strain in Voronoi lattices when degrees of cell regularity are varied.

For TWF, waviness effects on tensile properties and surface fracture behaviors of the resin between the interlacing tows were studied by Fujita *et al.* (1993). It was remarked that the TWF composites are isotropic in modulus, but anisotropic in strength, independent of tows orientation. This is in contrast to the biaxial woven fabric composites, which have a low shear resistance (Mallikarachchi and Pellegrino 2013). It was observed also that the direction of tow influences the fracture behaviors of the resin. In the examination of the effects of tow waviness, Kueh (2013) found that an increase in the initial waviness of the weave (skin) alone reduces the stiffness of the TWF composite sandwich structures, resulting in a drop in the global buckling load. A decline in the elastic modulus of TWF as a result of the tow waviness had also been noticed by Kueh (2012) and (2014) when investigating its mechanical properties by means of the wavy beam network and fitting-free hyperelastic strain energy models, respectively. To appreciate the importance of the tow waviness, Bai *et al.* (2016) used the strain energy micromechanical curved beam models to compute the tensile and shear moduli of TWF composite, which agree with the numerical and experimental results published by

Kueh and Pellegrino (2007). Mishra (2013), recognizing the importance of the tow waviness of TWF, predicted its in-plane mechanical behaviors by adopting a series of solid finite elements.

From the aforementioned literature review on lattices, it is vital to see that most of these studies focus on the fracture toughness of perfectly flat structures. The study on the effect of the waviness of structural members upon the fracture properties of the lattice remains absent. On the other hand, the majority of these investigations do not consider lattice with anisotropic members. Anisotropy of the members of TWF composite structure should be considered because the macroscopic strength of TWF is not isotropic although it is evidenced in its initial stiffness. Furthermore, a reduction in the tensile and compressive properties of TWF, due to the waviness of structural members, has been recognized in recent studies, as noted readily in the aforementioned review (Fujita *et al.* 1993, Kueh 2012, 2013, 2014). We, therefore, aim to explore the effects of tow waviness and anisotropy on the fracture toughness of TWF, focusing especially on the Mode II deformation, to address the research void.

The paper is arranged as follows. After the introductory section, the experimental and numerical techniques to evaluate the mechanical and fracture toughness properties of TWF are offered. In Section 3, the load-deformation and fracture behavior, as well as model verification, are presented. Then, the effects of waviness and anisotropic properties on the Mode II fracture toughness of single-ply TWF composite are explored and discussed. The concluding remarks, in the end, complete the paper.

2. Material and methods

2.1 Material

TWF in 'basic weave' pattern from Sakase Adtech, Japan, consisting of 1000-filament in each T300 carbon fiber tow (Toray Industries Inc., Japan) as well as the commercial epoxy resin, Epicote 1006, and hardener from S&N Chemicals Sdn Bhd, were used as the material. Epicote 1006 and hardener with the 5:3 proportions were mixed thoroughly with a mechanical stirrer for 30 seconds to produce the matrix. Vacuum bagging method was employed to prepare the TWF composite by first applying an equal distribution of matrix on both faces of a single-ply dry fabric. Excess matrix was next sucked into the bleeder

cloth by vacuuming. The lay-up was then cured in the room temperature of 25°C for 4 hours.

2.2 Experiment

Mechanical properties for the constituents of TWF, fibers and matrix, were first obtained. The experimental tensile tests were conducted for 5 dog bone shaped samples of the neat matrix, Epicote 1006, employing the testing standard ASTM D638 (ASTM 2010). The properties are listed in Table 1. In addition, the properties of T300 carbon fiber offered in the same table were taken from literature. Furthermore, the tensile strength of single tow T300/Epicote 1006 composite and the fracture toughness of single-ply TWF composite were next experimentally measured.

2.2.1 Tensile test of single tow

T300/ Epicote 1006 composite

Tensile test was conducted for three specimens of T300/Epicote 1006 composite tow of width 0.974 mm and thickness 0.0835 mm according to ASTM D3039 (ASTM, 2000). The tows were cut to a length of 250 mm. In addition, two carbon fiber composite plates of 50 mm × 10 mm × 0.426 mm were glued using the industrial superglue to both ends of each specimen, acting as tabs sandwiching the single tow sample to prevent any slippage and premature failure during the test (see Fig. 2). Then, each sample was installed into the Instron machine 5567 and pulled until failure with a loading rate of 0.2 mm/min. The average measured tensile strength of the composite tow was determined as 608 MPa.

2.2.2 Fracture toughness testing method

The fracture toughness test under Mode II loading was conducted according to the method originally proposed by Richard (1984) and adopted later by Jamali (2014). In general, the fracture toughness is a function of crack size, load, and geometry. The shape factor, Y , as a function of the crack length, a , and the specimen width, w , is used to derive the expressions for the Mode II fracture toughness, given as the followings

$$K_{IIc} = Y_{II} \sigma_{IIc} \sqrt{\pi a}$$

where

$$Y_{II} = \sin \alpha \frac{1}{1 - \frac{a}{w}} \sqrt{\frac{-0.23 + 1.4 \left(\frac{a}{w-a}\right)}{1 - 0.67 \left(\frac{a}{w-a}\right) + 2.08 \left(\frac{a}{w-a}\right)^2}} \quad (1)$$

Table 1 Properties of T300 carbon fiber and Epicote 1006 matrix

Property	T300 carbon fiber	Epicote1006 matrix
Density, ρ (kg/m ³)	1,760	1,273
Longitudinal extensional modulus, E_1 (MPa)	230,000	2,646
Transverse extensional modulus, E_2 (MPa)	14,000	2,646
In-plane shear modulus, G_{12} (MPa)	8,960	935
Major in-plane Poisson's ratio, ν_{12}	0.2	0.41
Minor in-plane Poisson's ratio, ν_{21}	0.01	0.41
Tensile strength (MPa)	3,530	47

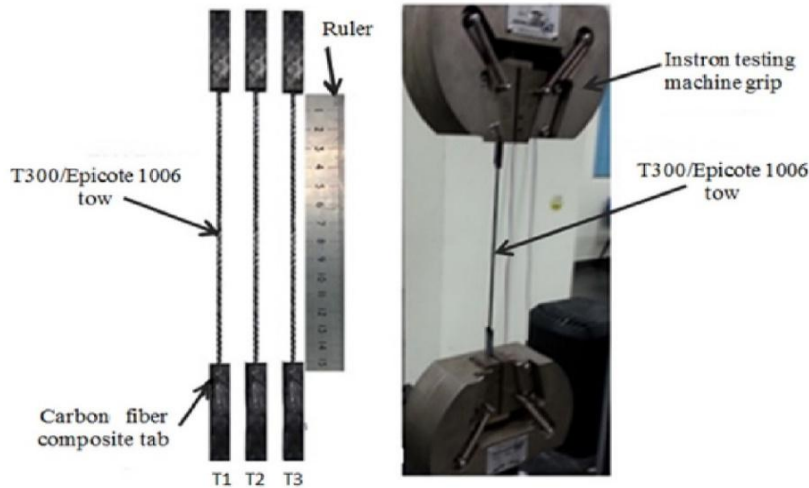


Fig. 2 (a) Specimens of T300/Epicote 1006 composite tow sandwiched by two carbon fiber composite plates for the tensile test; (b) Installation of specimen onto the machine grips

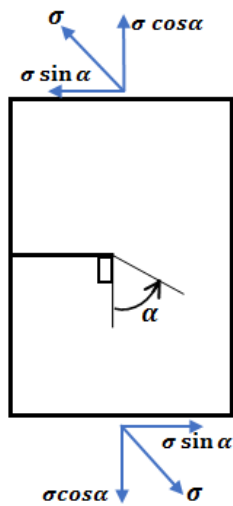


Fig. 3 Specimen configuration with an initially notched crack and the definition of loading angle, α (for Mode II loading, $\alpha = 90^\circ$)

σ_{IIC} is the critical Mode II stress that causes the first crack growth, w defines the specimen width, and a is the edge crack length. The loading angle is described as $\alpha = 90^\circ$ in Eq. (1), see Fig. 3. Note that the effect of the shape factor on K_{IIC} is rather small for the range of a/w studied although this does not apply to K_{IC} (Choupani 2008).

Since the single-ply TWF composite specimen is ultrathin and lightweight, a modified fixture as shown in Fig. 4, for the so-called compact tensile shear test coupon configuration previously used by Jamali (2014) for K_{IIC} determination, was implemented using aluminum plates of 1 mm thickness. Two aluminum plates were used at the top and the bottom sections of the specimen. A thicker section close to the end of fixture was provided by gluing another set of aluminum plates in order to eliminate the bending moment effect in the gripped area.

Five different edge crack lengths, a , of 5.4 mm, 8.1 mm, 10.8 mm, 14.85 mm, and 18.9 mm were introduced separately to the single-ply TWF composite specimens. The specimens were cut into the dimensions of 59.4 mm \times 36

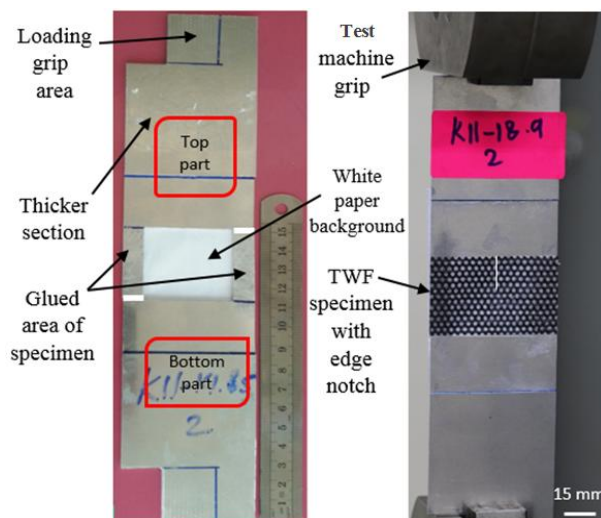


Fig. 4 (a) Modified fixture for Mode II test (without specimen); (b) Installation of specimen onto the fixture as well as the machine grips

mm as shown in Fig. 1. Three specimens for each crack length were tested. The specimens were first glued to the fixture, which was then installed to the Instron machine 5567 for the implementation of shear loading (see Figs. 4(b)). They were pulled until failure, at a room temperature of 25°C with a displacement rate of 0.5 mm/min. The load was measured by a 30 kN load cell. The fracture toughness of each specimen was calculated according to Eq. (1), by focusing on the first significant crack growth load for verification of numerical model. Also, the force versus loading head displacement was monitored for all specimens.

2.3 Numerical modeling

The TWF composite has an average thickness, h , of 0.167 mm, which was measured using the digital caliper with knife-edge jaws. For modeling convenience, an employment of rectangular cross-section with an average height of 0.0835 mm, which equals to a half of the average thickness of the cured composite, for the tow was utilized. In addition, the widths of our modeled tow cross section were varied, the values of which will be presented next in Section 2.3.1. The volume fraction of fiber within a tow was measured using the weighing method and determined for dry and cured materials as $V_f = 0.653$.

To study the waviness and anisotropy effects of TWF tows on Mode II fracture toughness, three types of model with associated features as categorized in Table 2 were considered. In Table 2, 2D planar isotropic Kagome and TWF isotropic models were used to investigate the waviness effect while those of TWF isotropic and TWF anisotropic were used to investigate the anisotropy effect. In addition, the effects of three parameters; relative density (t/l), cell size (l), and crack length (a) on fracture toughness were explored. The tow of the anisotropic model was assumed as a linear-elastic and transversely isotropic material, in which five independent elastic constants are needed (Isaac and Ishai 1994): the longitudinal extensional modulus, E_1 , the transverse extensional modulus, E_2 , the longitudinal Poisson’s ratio, ν_{12} , and the shear moduli, G_{12}

and G_{23} . While the tow of isotropic model was assumed as a linear-elastic material with only two independent elastic constants: stiffness, E , and Poisson’s ratio, ν . The computed engineering properties of T300/Epicote 1006 composite tow are summarized in Table 3.

2.3.1 Examined parameters

Table 4 summarizes the designated parameters covered by our models. Note that for all considered parameters, K_{IIc} were determined. The relative density of the TWF composite unit cell (see Fig. 1) is defined by the ratio of the cell wall thickness to cell size, t/l . Here, the fracture toughness for TWF composite of five different ratios of t/l as listed in Table 4 were modeled and calculated. In each t/l ,

Table 4 Summary of parameters considered for their effects on fracture toughness by means of finite element modeling

Effect	a (mm)	l (mm)	t (mm)	a/w	t/l	a/l
Relative density	18.9	1.56	0.947	0.538	0.607	12.11
	18.9	1.56	0.711	0.538	0.456	12.11
	18.9	1.56	0.473	0.538	0.303	12.11
	18.9	1.56	0.355	0.538	0.228	12.11
	18.9	1.56	0.236	0.538	0.151	12.11
Cell size	18.9	1.56	0.118	0.538	0.076	12.11
	9.45	0.78	0.947	0.538	1.214	12.11
	18.9	1.56	0.947	0.538	0.607	12.11
	37.8	3.12	0.947	0.538	3.294	12.11
Crack length	75.6	6.24	0.947	0.538	6.589	12.11
	2.7	1.56	0.947	0.077	0.607	1.73
	5.4	1.56	0.947	0.154	0.607	3.46
	8.1	1.56	0.947	0.231	0.607	5.19
	10.8	1.56	0.947	0.307	0.607	6.92
	13.5	1.56	0.947	0.384	0.607	8.65
	14.85	1.56	0.947	0.421	0.607	9.52
18.9	1.56	0.947	0.538	0.607	12.11	

Table 2 Three types of model with two comparison cases

Examined behavior	Type of model	Feature
waviness	2D planar isotropic Kagome	- Rigid connection with planar tows
		- Isotropic tows
anisotropy	TWF isotropic	- E, ν (Elastic constants)
		- Interweaving tows with beam-type connection
	TWF anisotropic	- Isotropic tows
		- E, ν (Elastic constants)
		- Interweaving tows with beam-type connection
		- Anisotropic tows
		- $E_1, E_2, \nu_{12}, G_{12}, G_{23}$ (Elastic constants)

Table 3 Properties of T300/Epicote 1006 composite tow

E_1 (MPa)	E_2 (MPa)	G_{12} (MPa)	G_{23} (MPa)	ν_{12}	ν_{23}
151,109	7,734	3,039	3,171	0.27	0.22

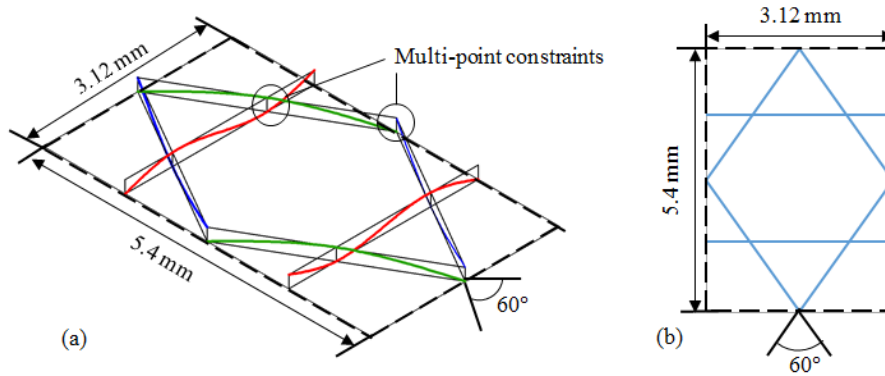


Fig. 5 Repeating unit cell for (a) 3D TWF and (b) 2D planar models

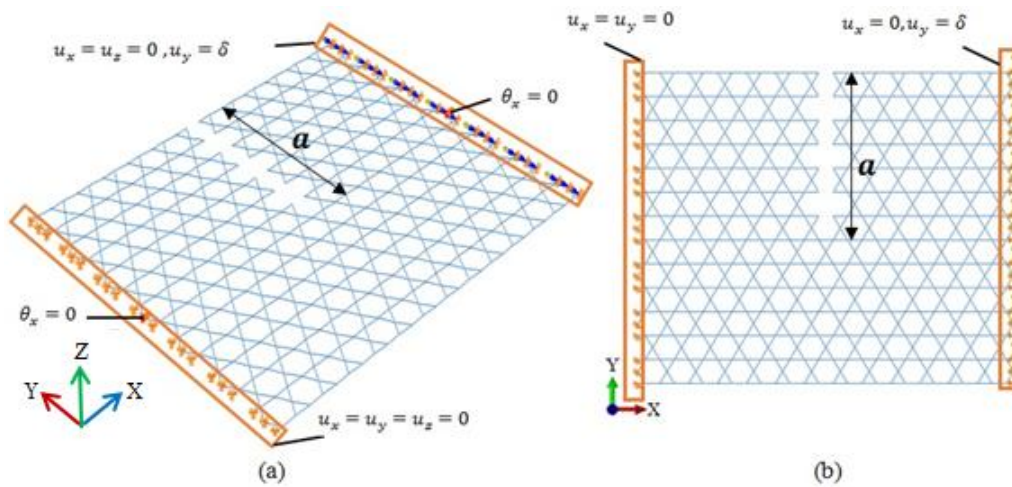


Fig. 6 Mode II modeling for (a) notched single ply TWF; and (b) notched 2D planar models

the crack length, a , and cell size, l , were held constant at $a = 18.9$ mm and $l = 1.56$ mm, respectively. In addition, the fracture toughness for TWF composite of four different cell sizes, l , were modeled and determined. The ratio of crack length to cell size, a/l , and the unit cell thickness, t , were held constant at $a/l = 12.11$ and $t = 0.947$ mm, respectively. In terms of the crack length effect, the cell size, l , and the relative density, t/l , were held constant at $l = 1.56$ mm and $t/l = 0.607$, respectively.

2.3.2 Finite element modeling of 2D planar Kagome lattice and single-ply TWF

The commercial finite element (FE) software, ABAQUS 6.13 (ABAQUS, 2013), was used to simulate the Mode II fracture toughness of TWF structure. All models were fixed to 13×7 cells with overall dimensions of 40.56 mm \times 35.1 mm. Three-dimensional network model employing a set of one-dimensional beam elements was used to capture the effects of tows waviness for the TWF anisotropic and TWF isotropic models, due to the interweaving nature of tows. Fig. 5 shows repeated unit cells used in the TWF and 2D planar Kagome modeling. Sine wave curved Euler-Bernoulli beam element, B31, was used to discretize the model with wavy members.

On the other hand, a 2D environment was used to simulate the 2D planar isotropic Kagome model adopting a

set of 2D flat Euler-Bernoulli beam elements, B21. Fig. 6 shows the 3D and 2D modeling for Mode II loading of TWF and 2D planar models, along with the applied loading types and boundary conditions. u_x , u_y , and u_z are the translations in the X-, Y-, and Z-directions, respectively, whereas θ_x , θ_y , and θ_z are the rotations about the X-, Y-, and Z-axes, respectively. The connectivity between the tows

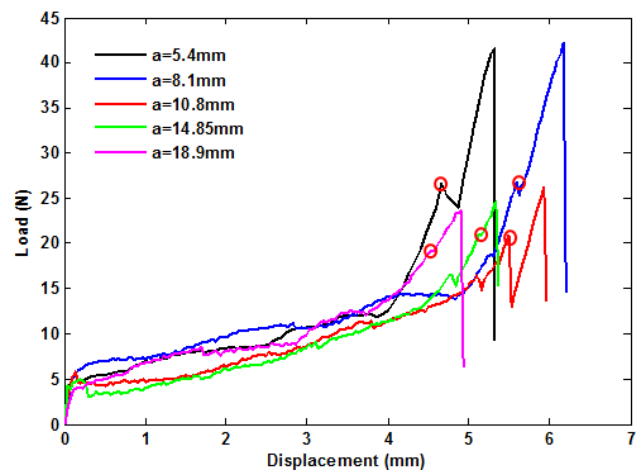


Fig. 7 Experimental load-displacement relationship of test specimens for Mode II loading

of TWF models was ensured by using the multi-point constraint function *MPC of beam type with translations and rotations synchronization between two linked nodes. Since the 2D planar isotropic Kagome model setting applied the assumption of a rigid connection at the intersections, no further constrain was described. The boundary conditions for 2D planar Kagome model were defined without the consideration of the out-of-plane components. The edge crack lengths, a , were produced by vanishing of beam elements with varying lengths.

The edge crack lengths were introduced for models according to Table 4. In all modeling, the geometrically

non-linear analysis was adopted. By assuming that the material, T300/ Epicote 1006, is linear elastic up to failure and the employed fracture stress, $\sigma_f = 608$ MPa (obtained from the single composite tow tensile tests), the fracture toughness of each model was calculated as follows. A known uniform shear stress, σ , was applied to the TWF model. Fracture happens when the maximum local stress anywhere in the model reaches the fracture stress, σ_f , at a certain applied remote stress ($\sigma = \sigma_{IIc}$). Using $\sigma = \sigma_{IIc}$, the fracture toughness was then calculated from Eq. (1) for Mode II with the consideration of $\alpha = 90^\circ$.

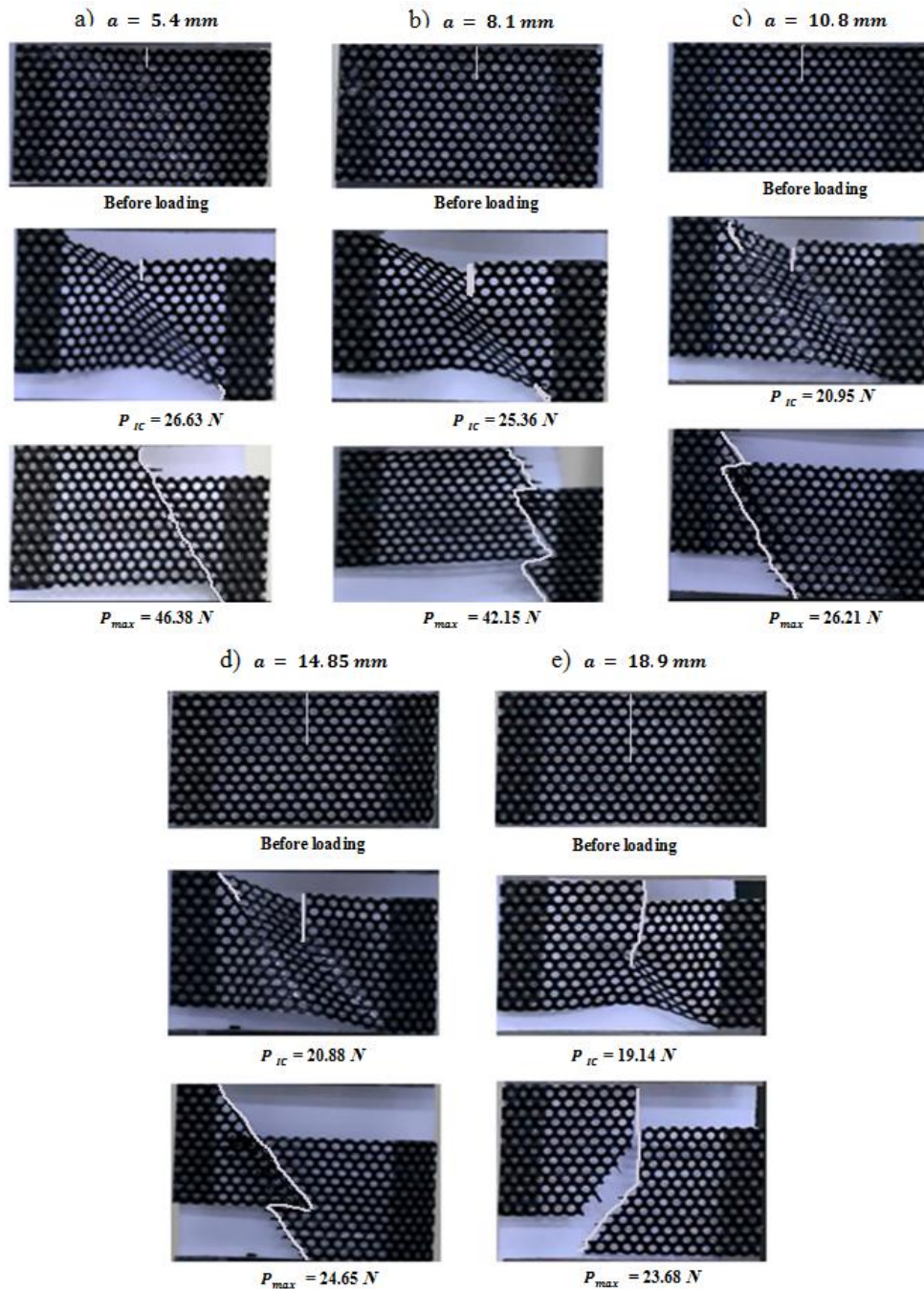


Fig. 8 A series of images showing the main crack growth in the TWF composite specimens during Mode II loading. The images correspond to load-displacement curves in Fig. 7 for crack lengths of (a) 5.4 mm; (b) 8.1 mm; (c) 10.8 mm; (d) 14.85 mm; and (e) 18.9 mm

3. Results and discussion

3.1 Load-deformation behavior

Fig. 7 shows typical force versus displacement relationships for Mode II tests for TWF specimens with initial cracks of 5.4 mm, 8.1 mm, 10.8 mm, 14.85 mm, and 18.9 mm. A small drop in the load-displacement curve before the maximum load point is observed in all specimens, indicating the first appearance of crack growth. The curves of Mode II in Fig. 7 show a non-linear behavior. They are in general divided into three main stages: Firstly, there is a steep linear load-displacement increment up to around 5N; the second stage exhibits a large displacement accompanied by little force increment. This is caused by the tendency of the TWF specimen to bend out-of-plane. It is noted that the extensive out-of-plane deformation occurred in specimens is clearly due to the fold ability and flexibility of TWF composite material. After that, loads in all specimens increase with little nonlinearity until the maximum failure

loads are reached. Then, they suddenly drop to zero. Note that due to low loading rate applied to all samples during testing, their load-deformation relationships were observed to be rather consistent and repeatable. Hence, only a representative curve is displayed in Fig. 7 for each sample. The stochastic nature of the load-displacement relationship, if it exists at all, is small in our case. It is the focus of this paper to determine the applied load value that causes the failure of the first member of the specimen during Mode II loading test, all of which are highlighted in Fig. 7 by small red circles on the curves. Note that this employed method had also been used in Fleck and Qiu (2007) although different geometries were considered by modeling approach only. It is clear that the stiffness and the maximum failure load of the specimen decrease when the crack length increases due to a reduction in remaining non-cracked members to resist the applied force.

Fig. 8 shows three images depicting the crack formation and progression in specimens for Mode II loading for differently examined crack lengths. In each set of three

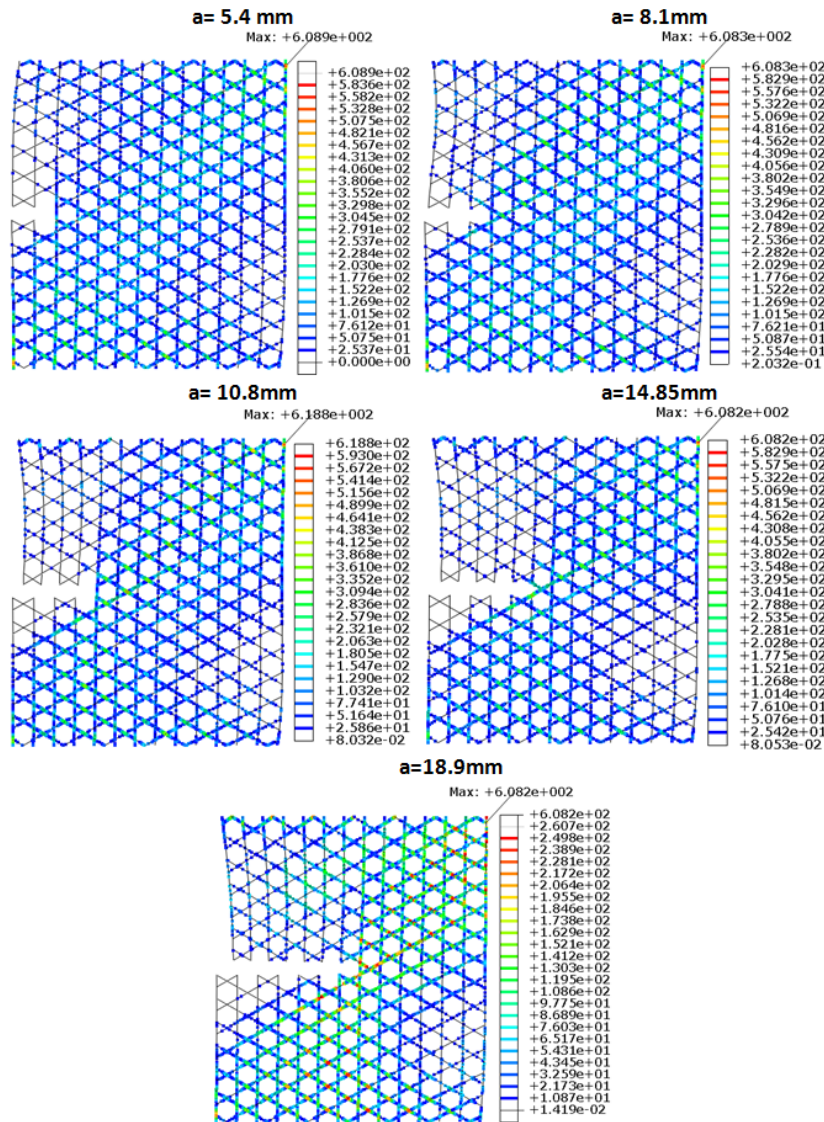


Fig. 9 Stress map for TWF anisotropic models highlighting the first failure locations with the maximum stress for various crack lengths

subfigures, the first image represents the specimen before loading, the second image corresponds to the small drop point in the load-displacement curve implying the initiation of crack propagation, and the third image correlates to the occurrence of the maximum load in the load-displacement curve. The distinct digitally whitened region visible in the second image in Fig. 8 displays the cracked location. It is clear that the first crack growth does not necessarily start in the area ahead of the crack-tip for the single-ply TWF composite material. Such observation had previously been noticed by Schmidt and Fleck (2001) for Mode I fracture toughness of regular aluminum alloy honeycomb foams, where they found that the cell walls that failed first were not located directly ahead of the crack tip because the maximum bending moments were achieved above and below the crack tip. Furthermore, the same observation had been seen by Christodoulou and Tan (2013) in lattices with different cell-regularities, mode-mixities, relative densities, and T-stresses. In their work, the crack initiation occurred at up to six cells from the crack tip in regions of high strain gradient and high localized strain, suggesting a highly discontinuous cracking path that is bridged by many uncracked ligaments.

Fig. 9 shows the stress map for TWF anisotropic models. Each subfigure presents the first failure location with the maximum stress value, which is at the top right corner near the support. The diagonally distributed high-stress region starts from its maximum location near support and progresses to the crack tip, i.e., the crack growth path, which replicates similarly that of the main crack growth in TWF composite test specimen as shown in Fig. 8. Thus, this confirms the applicability of the modeling assumption presented in Section 2.3.2, which states that the fracture happens when the maximum local stress anywhere in the model due to the applied remote uniform stress reaches the tensile strength of the single tow of the TWF structure. The fracture toughness is hence defined in this paper and that of Fleck and Qiu (2007) as when the tensile strength of any member is reached, regardless of its location. In the third image, the distinct digitally whitened region denotes the crack propagation path, which had clearly taken a tortuous route and ended up deviating away from that of the initial fracture. The crack path propagation was connected with the initially cracked line in the specimens with $a = 5.4$ mm

and 18.9 mm, where they propagated with a certain angle from the notch direction following the weakest path along one tow. For $a = 8.1$ mm, 10.8 mm, and 14.85 mm, the cracks started at the region near the support far away from the initially notched area, and also propagated with a certain angle following the weakest path along one tow. Examining closely, one can see that the angle that the crack deviated dominantly follows the tow direction, either 60° or -60° . This observation agrees with the fracture pattern shown in Kosugi *et al.* (2011) although their loading was of cyclic nature.

The deformation of the notched single-ply TWF model due to Mode II loading, illustrated in Fig. 10(a), shows that the tows bend slightly out-of-plane, which is similar to those seen in experimental specimens (see Fig. 8). This is due to the three-dimensional degree of freedom effects of single-ply TWF structure. In Fig. 10(b), the notched 2D planar model deforms by bar stretching in the area remote from the crack tip, but by a combination of bar stretching and bending within a characteristic elastic deformation zone near the crack tip. A similar deformation mode had been noticed in planar lattices and discussed by Romijn and Fleck (2007).

3.2 Model verification

The dependence of fracture toughness on the crack length to cell size ratio, a/l , was chosen to verify the FE results with those from experiments in Fig. 11. Note that only the TWF models with wavy and anisotropic beam elements were used in this comparison since they represent closely the experimentally studied material. The curves show that the behaviors of the modeled results replicate those of experiments.

The relationship between K_{IIC} and a/l progresses non-linearly, where K_{IIC} increases rapidly for $a/l < 6.92$, but with a reduced rate for greater a/l . Here, it is clear that K_{IIC} increases with a/l . In general, the fracture toughness obtained from experiments and models exhibit good agreements with up to 92% similarity. It is suspected that the small differences are attributed to some imperfections in TWF specimens used in the experimental work. Currently, material imperfections other than tows waviness are outside the scope of our study. For in-depth study on the sensitivity

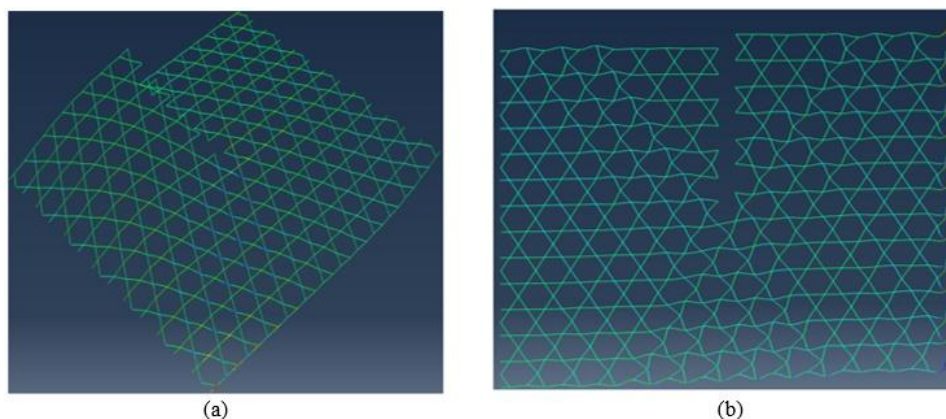


Fig. 10 Deformation due to Mode II loading for notched (a) single-ply TWF; and (b) 2D planar models

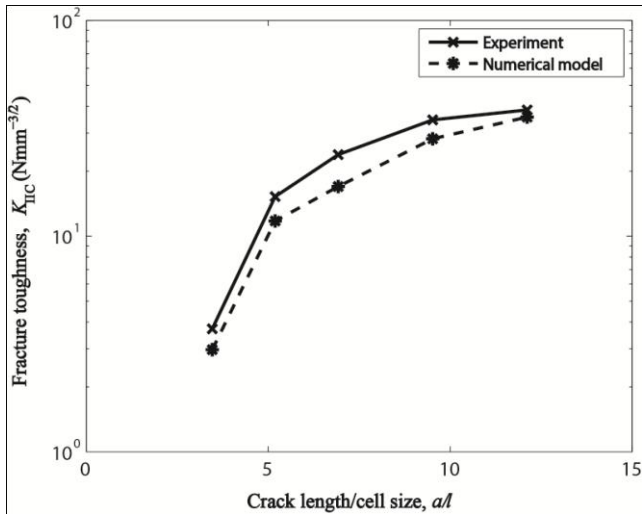


Fig. 11 Comparison between experimentally and numerically obtained dependence of K_{IIc} on a/l

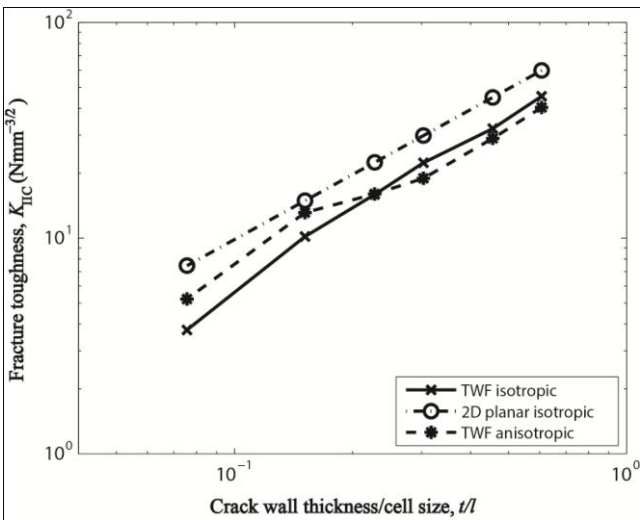


Fig. 12 Waviness and anisotropy effects on K_{IIc} for varying t/l

linear for the TWF isotropic and TWF anisotropic models. Mode II fracture toughness of TWF isotropic is lower than that of 2D planar model with differences between 24% - 32% for $t/l = 0.151 - 0.607$. Lower t/l shows a larger difference. The difference increases to around 50% for $t/l < 0.151$.

The TWF anisotropic model curve intersects with that of TWF isotropic at $t/l = 0.228$. K_{IIc} for TWF isotropic model is 24% lower than that of TWF anisotropic when $t/l < 0.151$. Then, it is 10% larger than that of TWF anisotropic model. It is noted that K_{IIc} scales with the relative density, t/l , according to the following expression

$$K_{IIc} = C_{II} \sigma_f \sqrt{l} (t/l)^{d_{II}} \quad (2)$$

where C_{II} is the intercept at the vertical axis for the logarithmic $K_{IIc}/\sigma_f \sqrt{l}$ versus $(t/l)^{d_{II}}$ relationship, which are 0.149, 0.113, and 0.129 for TWF anisotropic, TWF isotropic, and 2D planar Kagome, respectively, whereas the relationships are raised to the power, d_{II} , of 1.27, 1.17, and

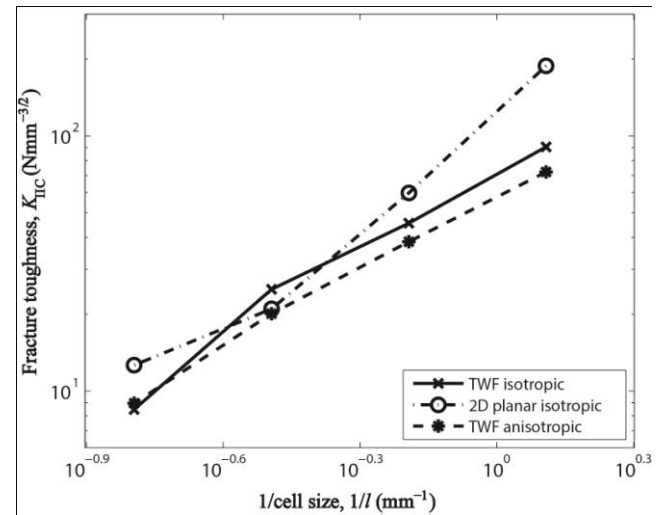


Fig. 13 Waviness and anisotropy effects on K_{IIc} for varying $1/l$

of fracture toughness on various material defects, work by Romijn and Fleck (2007) is referred. Nonetheless, the agreement between our modeled and experimental outcomes is clear since the general patterns of K_{IIc} vs a/l are closely replicated. The currently employed modeling technique is hence verified.

3.3 Effects of parametric changes on fracture toughness

Having verified the modeling technique, the dependence of Mode II fracture toughness on relative density, cell size, and crack length in terms of anisotropy and waviness of tow were further investigated using FE modeling. The obtained results are discussed below.

3.3.1 Dependence of fracture toughness on relative density

Fig. 12 shows that the relationship between K_{IIc} and t/l is linear for the 2D planar isotropic model, but slightly non-

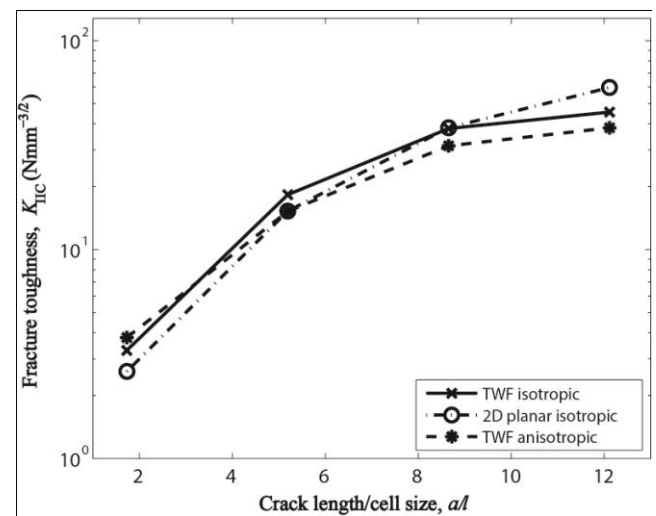


Fig. 14 Waviness and anisotropy effects on K_{IIc} for varying a/l

1.0, respectively. Overall, K_{IIC} increases with t/l . In general, the waviness produces lower K_{IIC} due to lowered tows stiffness as well as strength from three-dimensional unconstrained degrees of freedom effects, while isotropic and anisotropic materials show almost the same behavior. This behavior is aligned with those of Kueh (2013, 2014), in which a reduction in elastic mechanical properties was noticed if the members are of wavy form. The latter observation means the reduction of stiffness in the transverse direction due to anisotropic tows has little influence on the fracture toughness for numerous relative densities.

3.3.2 Dependence of fracture toughness on cell size

Fig. 13 shows the relationship between K_{IIC} and l/l due to waviness and anisotropy effects. The TWF isotropic and 2D planar models have two intersection points at $l/l = 0.25$ and 0.406. K_{IIC} of TWF isotropic model is greater than that of 2D planar within these values. The opposite is true outside this range with the percentage of difference reaching 50%. K_{IIC} of TWF anisotropic model is 20% lower than that of TWF isotropic model when $l/l \geq 0.320$. This percentage gradually decreases to zero when $l/l < 0.320$.

Again, it is apparent that K_{IIC} increases with l/l . In general, K_{IIC} of 2D planar models are greater than those of TWF because wavy tows lead to a decrease in resistance to crack. On the other hand, the reduction in the transverse stiffness of anisotropic tows decrease only slightly K_{IIC} when l/l is raised.

3.3.3 Dependence of fracture toughness on crack length

Fig. 14 shows a nonlinearity in K_{IIC} against a/l for all models. K_{IIC} of TWF isotropic model is averagely 20% greater than those of 2D planar model when $a/l \leq 8.65$, and the trend is reversed when $a/l > 8.65$. K_{IIC} of TWF isotropic model is slightly conforming with that of TWF anisotropic model when $a/l < 5.19$ and averagely 15 %

greater than that of TWF anisotropic model when $a/l > 5.19$.

In general, K_{IIC} increases with a/l . K_{IIC} of 2D planar model is still greater than that of TWF isotropic model, although its trend is reversed when $a/l < 8.65$. The plots show that K_{IIC} of TWF anisotropic and TWF isotropic models with varying crack lengths are approximately constant when a/l is greater than 8.1. For a/l less than 8.1, K_{IIC} decreases drastically. K_{IIC} of 2D planar Kagome model is increasing rapidly for all varying crack lengths though with some softening effect when $a/l > 5.19$.

By considering the maximum K_{IIC} at $a/l = 12.11$ for 2D planar and constant K_{IIC} at $a/l > 8.1$ for TWF anisotropic and TWF isotropic models, a reduction factor, β , can be determined by dividing all K_{IIC} by these associated values. The reduction factors are plotted in Fig. 15 and can be approximated by

$$\beta = 1 - \exp[A(a/l)^B] \quad (3)$$

from which $A = -0.016$ and -0.024 as well as $B = 2.12$ and 2.1 for 2D planar and TWF models, respectively. The effective fracture toughness can then be expressed with the reduction factor, β , as

$$K_{IIC} = \beta Y_{II} \sigma_{IIC} \sqrt{\pi a} \quad (4)$$

It seems that a reduction trend to a constant can be noticed in TWF models when a/l is greater than 8.1 although it is not so apparent that such a constant value is achieved for the 2D planar model within the range currently studied. Generally, tow waviness lowers K_{IIC} in all cases, due to a reduction in stiffness and strength. K_{IIC} of TWF isotropic is generally slightly greater than those of TWF anisotropic model. This is again attributed to the reduction in the transverse stiffness of anisotropic tows.

4. Conclusions

Tows waviness and anisotropy effects on Mode II fracture toughness of single-ply TWF composite were investigated by means of numerical and experimental methods. In terms of the load-displacement relationship, the specimens under Mode II loading exhibited some non-linear behavior initially with a large displacement due to out-of-plane bending. Then, the relationship is linear up to a global fracture state.

Three types of model: 2D planar isotropic Kagome, TWF isotropic, and TWF anisotropic were considered in the numerical work. 2D planar isotropic Kagome and TWF isotropic were used to investigate the waviness effect while TWF isotropic and TWF anisotropic models were for studying anisotropy effect. Having TWF anisotropic models verified with those experimentally measured, the dependence of fracture toughness on relative density (t/l), cell size parameter (l/l), and crack length to cell size ratio (a/l), were explored for all models, using the first crack growth load.

To sum up, a huge knockdown in the Mode II fracture toughness, up to 50%, was observed due to the effect of waviness for numerous relative densities and cell sizes. This

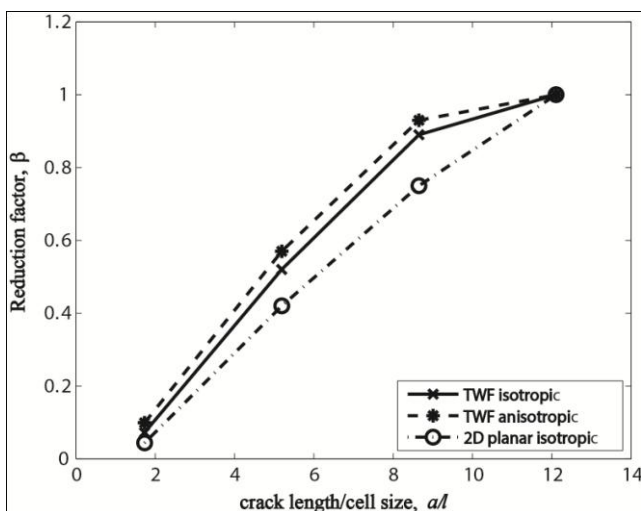


Fig. 15 Reduction factor for the three models due to varying a/l

lower resistance to crack propagation is attributed to the weakening of TWF by unconstrained three-dimensional degrees of freedom in all tows. For different a/l , such waviness effects in K_{IIC} are somewhat absent when $a/l < 8.65$. Due to anisotropy, K_{IIC} are generally only slightly higher in isotropic models, implying the type of material affects very little the fracture toughness of TWF.

Acknowledgments

The authors thank the Malaysian Ministry of High Education (MOHE) and Universiti Teknologi Malaysia for research grants (R.J13000.7809.4F518, Q.J130000.2522.17H92) and facilities.

References

- ABAQUS Version 6.13 (2013), Analysis User's Guide, Dassault Systems.
- Al-Fasih, M.Y., Kueh, A.B.H., Abo Sabah, S.H. and Yahya, M.Y. (2017), "Influence of tows waviness and anisotropy on effective Mode I fracture toughness of triaxially woven fabric composites", *Eng. Fract. Mech.*, **182**, 521-536.
- Alonso, I.Q. and Fleck, N. (2009), "The damage tolerance of a sandwich panel containing a cracked honeycomb core", *J. Appl. Mech.*, **76**(6), 061003-1-8.
- Aoki, T., Yoshida, K. and Watanabe, A. (2007), "Feasibility study of triaxially-woven fabric composite for deployable structures", *Proceedings of the 48th AIAA/ASME/ASCE/AHS/ASC Structures, Structural Dynamics and Materials Conference*, Honolulu, HI, USA, April.
- ASTM D638 (2010), Standard test method for tensile properties of plastics; ASTM International, West Conshohocken, PA, USA.
- ASTM D3039 (2000), Standard test method for tensile properties of polymer matrix composite materials; ASTM International, West Conshohocken, PA, USA.
- Bai, J., Xiong, J., Liu, M. and Man, Z. (2016), "Analytical solutions for predicting tensile and shear moduli of triaxial weave fabric composites", *Acta Mech. Solida Sin.*, **29**(1), 59-77.
- Baier, H. and Datashvili, L. (2011), "Active and morphing aerospace structures-A synthesis between advanced materials, structures and mechanisms", *Int. J. Aeronaut. Space Sci.*, **12**(3), 225-240.
- Choi, S. and Sankar, B.V. (2005), "A micromechanical method to predict the fracture toughness of cellular materials", *Int. J. Solids Struct.*, **42**(5), 1797-1817.
- Choupani, N. (2008), "Experimental and numerical investigation of the mixed-mode delamination in Arcan laminated specimens", *Mat. Sci. Eng. A-Struct.*, **478**(1), 229-242.
- Christodoulou, I. and Tan, P. (2013), "Crack initiation and fracture toughness of random Voronoi honeycombs", *Eng. Fract. Mech.*, **104**, 140-161.
- Erfani, S. and Akrami, V. (2016), "Evaluation of cyclic fracture in perforated beams using micromechanical fatigue model", *Steel Compos. Struct.*, *Int. J.*, **20**(4), 913-930.
- Fleck, N.A. and Qiu, X. (2007), "The damage tolerance of elastic-brittle, two-dimensional isotropic lattices", *J. Mech. Phys. Solids*, **55**(3), 562-588.
- Fujita, A., Hamada, H. and Maekawa, Z. (1993), "Tensile properties of carbon fiber triaxial woven fabric composites", *J. Compos. Mater.*, **27**(15), 1428-1442.
- Ho, S., Sheng, S. and Ouellette, P. (2003), "Determination of elastic properties of triax composite materials", *Compos. Sci. Technol.*, **63**(3), 437-443.
- Huang, J. and Gibson, L. (1991a), "Fracture toughness of brittle foams", *Acta Metall. Mater.*, **39**(7), 1627-1636.
- Huang, J. and Gibson, L. (1991b), "Fracture toughness of brittle honeycombs", *Acta Metall. Mater.*, **39**(7), 1617-1626.
- Isaac, M.D. and Ishai, O. (1994), *Engineering Mechanics of Composite Materials*, Oxford.
- Jamali, J. (2014), "Mechanistic failure criterion for unidirectional and random fibre polymer composites", Ph.D. Thesis; The University of Western Ontario, London, ON, Canada.
- Kosugi, Y., Aoki, T. and Watanabe, A. (2011), "Fatigue characteristic and damage accumulation mechanism of triaxially-woven fabric composite", *Proceedings of the 52nd AIAA/ASME/ASCE/AHS/ASC Structures, Structural Dynamics and Materials Conference*, Denver, CO, USA, April.
- Kueh, A.B.H. (2012), "Fitting-free hyperelastic strain energy formulation for triaxial weave fabric composites", *Mech. Mater.*, **47**, 11-23.
- Kueh, A.B.H. (2013), "Buckling of sandwich columns reinforced by triaxial weave fabric composite skin-sheets", *Int. J. Mech. Sci.*, **66**, 45-54.
- Kueh, A.B.H. (2014), "Size-influenced mechanical isotropy of singly-plyed triaxially woven fabric composites", *Compos. Pt. A-Appl. Sci. Manuf.*, **57**, 76-87.
- Kueh, A.B.H. and Pellegrino, S. (2007), "ABD matrix of single-ply triaxial weave fabric composites", *Proceedings of the 48th AIAA Structures, Structural Dynamics and Materials Conference*, Honolulu, HI, USA, April.
- Lee, S.-J., Wang, J. and Sankar, B.V. (2007), "A micromechanical model for predicting the fracture toughness of functionally graded foams", *Int. J. Solids Struct.*, **44**(11), 4053-4067.
- Lipperman, F., Ryvkin, M. and Fuchs, M.B. (2007), "Fracture toughness of two-dimensional cellular material with periodic microstructure", *Int. J. Fract.*, **146**(4), 279-290.
- Mallikaratchi, H. and Pellegrino, S. (2013), "Failure criterion for two-ply plain-weave CFRP laminates", *J. Compos. Mater.*, **47**(11), 1357-1375.
- Mishra, R. (2013), "Meso-scale finite element modeling of triaxial woven fabrics for composite in-plane reinforcement properties", *Text. Res. J.*, **83**(17), 1836-1845.
- Richard, H. (1984), "Some theoretical and experimental aspects of mixed mode fractures", In: (S.R. Valluri Editor), *Advances in Fracture Research*, Oxford: Pergamon Press, pp. 3337-3344.
- Rizov, V.I. (2017), "Non-linear study of mode II delamination fracture in functionally graded beams", *Steel Compos. Struct., Int. J.*, **23**(3), 263-271.
- Romijn, N.E. and Fleck, N.A. (2007), "The fracture toughness of planar lattices: Imperfection sensitivity", *J. Mech. Phys. Solids*, **55**(12), 2538-2564.
- Schmidt, I. and Fleck, N. (2001), "Ductile fracture of two-dimensional cellular structures—Dedicated to Prof. Dr.-Ing. D. Gross on the occasion of his 60th birthday", *Int. J. Fract.*, **111**(4), 327-342.
- Thiyagasundaram, P., Wang, J., Sankar, B.V. and Arakere, N.K. (2011), "Fracture toughness of foams with tetrakaidecahedral unit cells using finite element based micromechanics", *Eng. Fract. Mech.*, **78**(6), 1277-1288.
- Toribio, J. and Ayaso, F.J. (2003), "A fracture criterion for high-strength steel structural members containing notch-shape defects", *Steel Compos. Struct., Int. J.*, **3**(4), 231-242.
- Xu, D., Ganesan, R. and Hoa, S.V. (2007), "Buckling analysis of tri-axial woven fabric composite structures subjected to bi-axial loading", *Compos. Struct.*, **78**(1), 140-152.
- Zhao, Q. and Hoa, S. (2003), "Thermal deformation behavior of triaxial woven fabric (TWF) composites with open holes", *J. Compos. Mater.*, **37**(18), 1629-1649.
- Zhao, Q. and Hoa, S. (2005), "Finite element modeling of a

membrane sector of a satellite reflector made of triaxial composites”, *J. Compos. Mater.*, **39**(7), 581-600.

CC

Nomenclature

a	edge crack length
A, B	coefficients for reduction factor
CTS	compact tensile shear
E_i	extensional modulus, $i = 1, 2, 3$
G_{ij}	shear modulus, $i, j = 1, 2, 3$
h	average thickness of specimen
K_{IIC}	Mode II fracture toughness
l	cell size
L	total length of specimen
MPC	multi-point constraint
t	wall thickness of TWF unit cell
TWF	triaxially woven fabric composite
u_i	displacement, $i = X, Y, Z$ -axes
V_f	volume fraction of fiber
w	width of specimen
α	loading angle
β	reduction factor
ν_{ij}	Poisson's ratio, $i, j = 1, 2, 3$
θ_i	rotation, $i = X, Y, Z$ -axes
σ	shear stress
σ_f	fracture stress
σ_{IIC}	critical Mode II stress